J Mater Sci: Mater Electron (2021) 32:13539–13548

Effects of NiO addition on structure and dielectric properties of $BaTiO_3$-based ceramics

Qi Xu[1,*], Wanting Huang[1], Rui Deng[1], Hanxing Chen[2], and Hanxing Liu[2]

[1] College of Materials and Chemistry & Chemical Engineering, Chengdu University of Technology, Chengdu 610059, China
[2] State Key Laboratory of Advanced Technology for Materials Synthesis and Processing, School of Material Science and Engineering, Wuhan University of Technology, Wuhan 430070, China

Received: 21 January 2021
Accepted: 6 April 2021
Published online:
20 April 2021

ABSTRACT

The phase structure, microstructure, ferroelectric and dielectric properties of NiO-modified $BaTiO_3$-4.0 mol%Nb_2O_5 ceramics (BT-Nb-Ni) were systematically investigated. All the specimens revealed cubic perovskite structure along with $Ba_3Nb_{3.2}Ti_5O_{21}$ second phase by XRD analysis. Small amount of NiO addition ($x \leq 0.5$) had the effect of inhibiting grain growth, while a further increase of NiO content ($x \geq 1.0$) led to relatively large grains with an average grain size of $\sim$ 0.40 μm. From P-E hysteresis loops and modified Curie–Weiss fitting, NiO addition first reduced and then enhanced the relaxor behaviour of the system. The ε_r-T curves of BT-Nb-Ni ceramics were significantly flattened, leading to greatly optimized dielectric temperature stability. The optimum property was achieved in the composition BT-Nb-2.0%Ni with $\varepsilon_r = 1380$ and $\triangle C/C_{25\ ^\circ C} \leq \pm 15\%$ in the temperature range of − 65–170 °C.

1 Introduction

With the rapid development of electronic industry, multi-layer ceramic capacitors (MLCCs) have been increasingly used in electronic products such as mobile phones and personal computers. MLCCs are developing towards miniaturization, high reliability and low loss. The existing EIA (Electronic Industries Alliance) -X7R products can no longer satisfy the increasingly high requirements, especially in harsh temperature working conditions. Consequently, accelerating the exploration and application of dielectrics which are able to withstand higher temperature has attracted extensive attention.

$BaTiO_3$ system has been proved to be environmentally friendly material for the preparation of large-capacity MLCCs. However, the sharp decrease of permittivity above the Curie temperature makes it difficult to satisfy the R characteristics ($\triangle C/C_{25\ ^\circ C} \leq \pm 15\%$) when temperature is higher than 130 °C [1]. $BaTiO_3$-Nb_2O_5 system has been extensively studied as the candidate for MLCC dielectrics [2]. According to Sun [3] and Yao [4], after the addition of Nb_2O_5, the dielectric constant-temperature curves show two dielectric maxima instead of one single Curie peak. Due to the two-peak ε_r-T curves, Nb_2O_5 doped $BaTiO_3$ ceramics is more benefit for obtaining favorable dielectric-temperature stability. However,

Address correspondence to E-mail: xuqi17@cdut.edu.cn

https://doi.org/10.1007/s10854-021-05930-6

it is still difficult to obtain XnR compliant components by Nb_2O_5 doping alone. To further broaden the working temperature range, incorporation of complex oxides in $BaTiO_3$-based matrix has been proved to be effective, such as $BaTiO_3$-Nb_2O_5-Co_3O_4 [5], [$BaTiO_3$-$Bi(Mg_{1/2}Ti_{1/2})O_3$]- Nb_2O_5-Co_3O_4 [6], [$BaTiO_3$- $(Bi_{0.5}Na_{0.5})TiO_3$]-Nb_2O_5-Pr_6O_{11} [7] et al.

In this paper, we chose $BaTiO_3$-4.0 mol%Nb_2O_5 (BT-Nb) as the matrix [8], introducing NiO as the second oxide member. $BaTiO_3$-4 mol%Nb_2O_5-xmol%NiO (BT-Nb-xNi, x = 0, 0.5, 1.0, 2.0, 3.0) ceramics were prepared and the dielectric properties were investigated.

2 Experimental procedure

BT-Nb-xNi ceramics were prepared by conventional solid state reaction method. $BaTiO_3$ (0.4 μm, ≥ 99.9%), NiO (≥ 99.9%), Nb_2O_5 (≥ 99.5%) powders were mixed stoichiometrically and ball milled with zirconium media in ethanol for 24 h. After dried, the powder mixture were blended with 2.5 w.t% PVA solution, then pressed into pellets with ~ 12 mm in diameter and ~ 1 mm in thickness under a uniaxial pressure of 200 MPa. The organic binder was burnt off at 600 °C for 30 min.

The bulk density of the sintered ceramic samples was tested using the Archimedes principle. Phase structure was determined using X-ray powder diffractometer (Cu Kα radiation, Philips X′Pert ProMPD, Holland). Microstructure was studied by scanning electron microscope (JSM-5610LV, JEOL Ltd., Japan). Electrodes were fabricated with fire-on silver paste at 500 °C for 15 min. To determine the ferroelectric properties, the sintered samples were polished to a thickness of 0.3 (± 0.02) mm and then the test was performed using a ferroelectric testing system (HVI0403-239, Radiant Technology, USA) in a silicone oil bath at the frequency of 10 Hz. The dielectric properties were measured using a customer designed furnace connected to a precision LCR meter (E4980A, Agilent, USA) and computerized controlled data collection systems, with a heating rate of 2 °C/min.

3 Results and discussion

Table 1 lists the optimum sintering temperature and bulk density of BT-Nb-xNi ceramic samples. For x = 0 and 0.5 samples, the maximum density was obtained at the sintering temperature of 1225 °C. The ceramic samples with higher NiO content (x = 1.0–3.0) exhibited the maximum bulk density at the sintering temperature of 1250 °C. The bulk density value of each sample at the optimum sintering temperature was above 5.7 g/cm^3, showing good compactness.

Figure 1 shows the XRD patterns of BT-Nb-xNi ceramics sintered at optimum sintering temperature for 2 h. A homogeneous cubic perovskite structure was developed in all the specimens, but peaks for $Ba_3Nb_{3.2}Ti_5O_{21}$ second phase indicated by the rhombuses were also found. The emergence of this secondary phase might be attributed to the reaction between the displaced Ti^{4+} and redundant Nb^{5+} which did not completely enter into the $BaTiO_3$ crystal lattice.

The microstructure of BT-Nb-xNi ceramics was investigated by means of SEM, as illustrated in Fig. 2. All the samples were thermal etched at 1125–1150 °C beforehand and the images were taken from fresh cross sections. All the samples revealed a dense microstructure with well-developed grains and clearly visible grain boundaries. The average grain size of pure BT-Nb ceramics without NiO addition was calculated to be 0.36 μm. When NiO was added (x = 0.5), the grains tended to become smaller and part of the grain size decreased to 0.25 to 0.33 μm. It was in accordance with literature reports [9] that small amount of Ni^{2+} addition had the effect of inhibiting grain growth in $BaTiO_3$ based ceramics. With the further increase of NiO content, the ceramic grains had a tendency to grow again. The average grain size was determined to be 0.40 μm, 0.39 μm, 0.40 μm for the sample x = 1.0, 2.0, 3.0, respectively. This may be related to the formation of the secondary phase, which was proved by XRD analysis. However, it was hard to observe obvious grains of the impurity phase by SEM due to their minute quantity.

To figure out the ferroelectric properties of BT-Nb-xNi ceramics, the P-E hysteresis loops under different electric field were tested, as shown in Fig. 3. A pre-cycle was performed before the measurement. BT-Nb ceramics without NiO addition exhibited typical P-E loop of relaxor ferroelectrics with maximum

Table 1 Sintering temperature and bulk density for each composition

Sample	Composition $BaTiO_3$-4 mol%Nb_2O_5-xmol%NiO	Sintering temperature (°C)	Bulk density(g/cm^3)
1	$x = 0$	1225	5.73
2	$x = 0.5$	1225	6.08
3	$x = 1.0$	1250	5.86
4	$x = 2.0$	1250	5.86
5	$x = 3.0$	1250	5.72

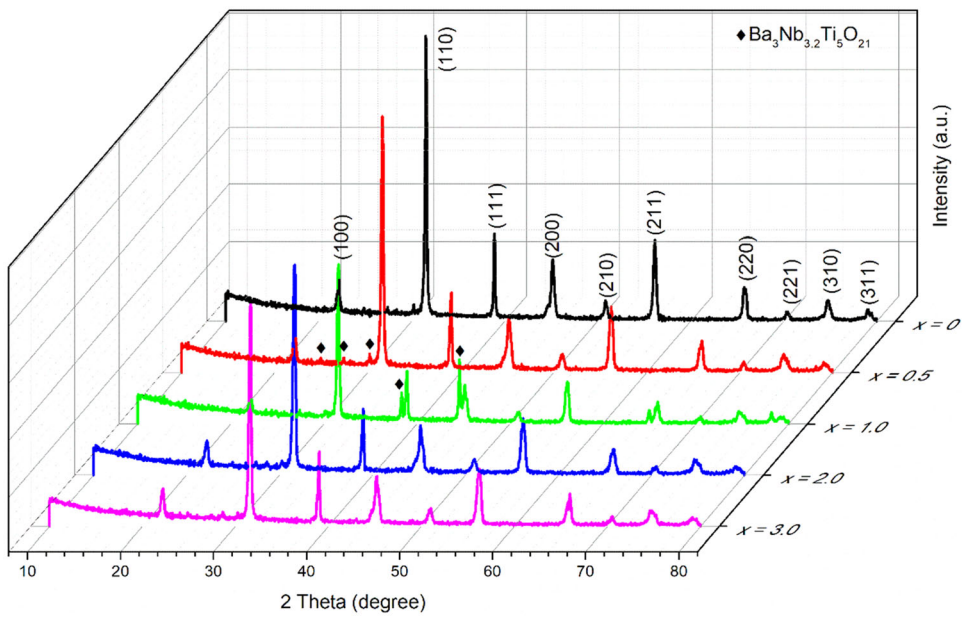

Fig. 1 XRD patterns of $BaTiO_3$-4 mol%Nb_2O_5-xmol%NiO ceramic samples

polarization P_m = 15.31 μC/cm^2 and residual polarization P_r = 5.51 μC/cm^2 under 8 kV/mm. With the introduction of NiO, the relaxor characteristics were greatly reduced, especially in the composition of $x = 0.5$ and $x = 1.0$. They represented more "fatter" hysteresis loops with large residual polarization intensity, as shown in Fig. 3b, c and f. However, further increase of NiO content led to slim loops instead. In the sample $x = 2.0$, the residual polarization (P_r) and coercive field (E_c) reduced to 2.94 μC/cm^2 and 1.14 kV/mm under an applied electric field of 8 kV/mm, respectively. The variation of relaxation characteristics in BT-Nb-xNi ceramics with NiO content can also be proved by the following analysis.

Figure 4 presents the dielectric constant and dielectric loss versus temperature for five groups of ceramic samples at different frequencies. As shown in Fig. 4a, two dielectric peaks can be observed at $T_1 \sim 40$ °C and $T_m \sim 140$ °C respectively in the composition BT-Nb ($x = 0$). It was demonstrated to be related to the formation of a chemically inhomogeneous structure [10]. After adding NiO, the dielectric constant of the system decreased as a whole. The low temperature end of the curve was flattened while the two peaks still existed. The first dielectric peak gradually shifted to higher temperature (T_1 = 52 °C → 53 °C → 60 °C → 63 °C for $x = 0.5, 1.0, 2.0, 3.0$), while the curie peak remained around 140 °C. It was supposed that when NiO and Nb_2O_5 were doped as composite oxide, Ni^{2+} and Nb^{5+} cations would substitute the Ti^{4+} sites by forming the $(Ni_{1/3}Nb_{2/3})^{4+}$ [9]. In this situation, Ni^{2+} and Nb^{5+} ions were more likely to diffuse into the crystal lattice in the form of $(Ni_{1/3}Nb_{2/3})^{4+}$ according to solubility analysis. As a result, the chemically inhomogeneous structure would form more easily and reflect as double peaks in the permittivity curves.

It can also be observed from Fig. 4 that all BT-Nb-xNiO samples exhibited obvious frequency dispersion and diffuse behavior, which were regarded as the typical characteristics of relaxor ferroelectrics

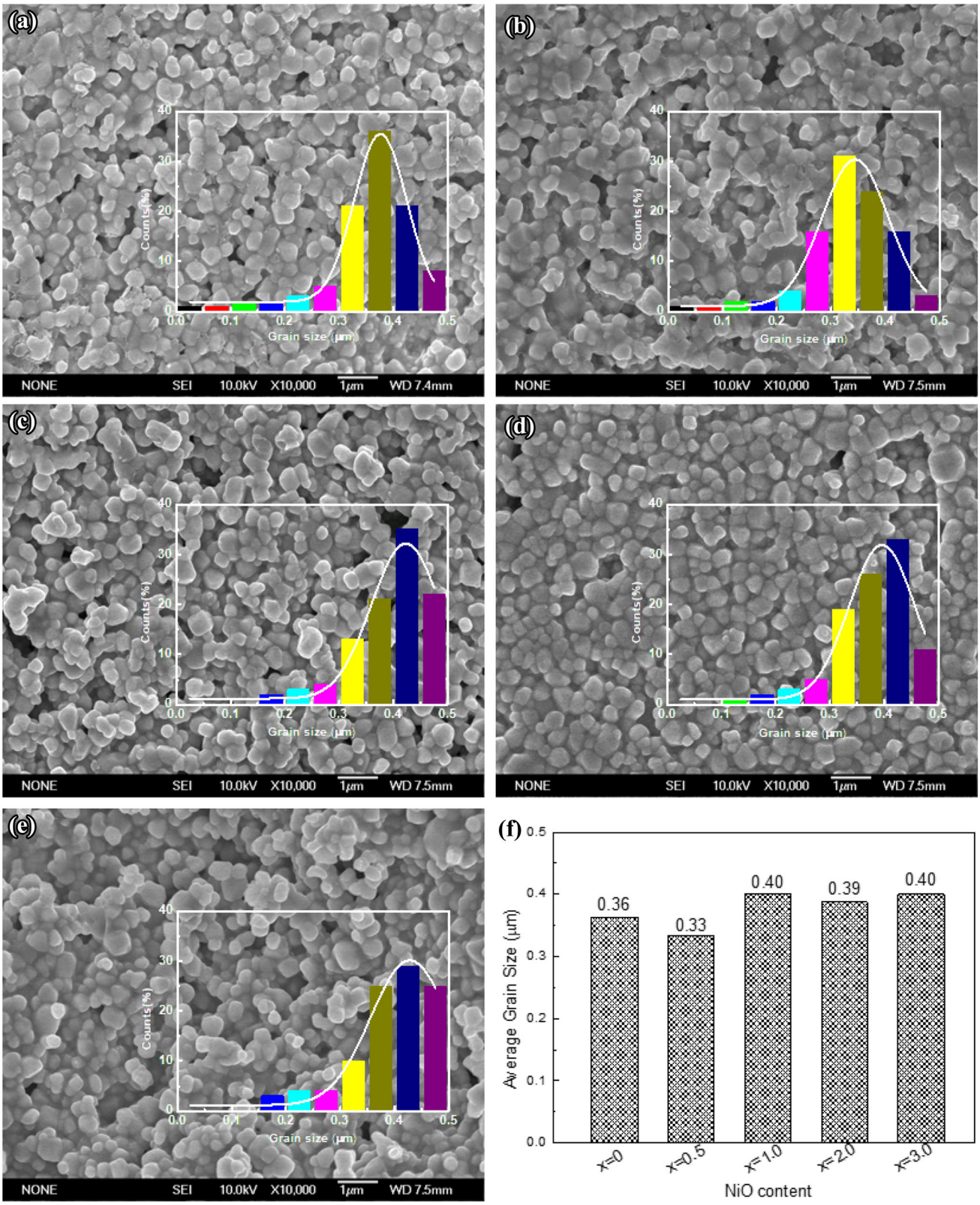

Fig. 2 Cross-section SEM images and calculated grain sizes of $BaTiO_3$-4 mol%Nb_2O_5-xmol%NiO ceramics: **a** $x = 0$, **b** $x = 0.5$, **c** $x = 1.0$, **d** $x = 2.0$, **e** $x = 3.0$, **f** average grain size

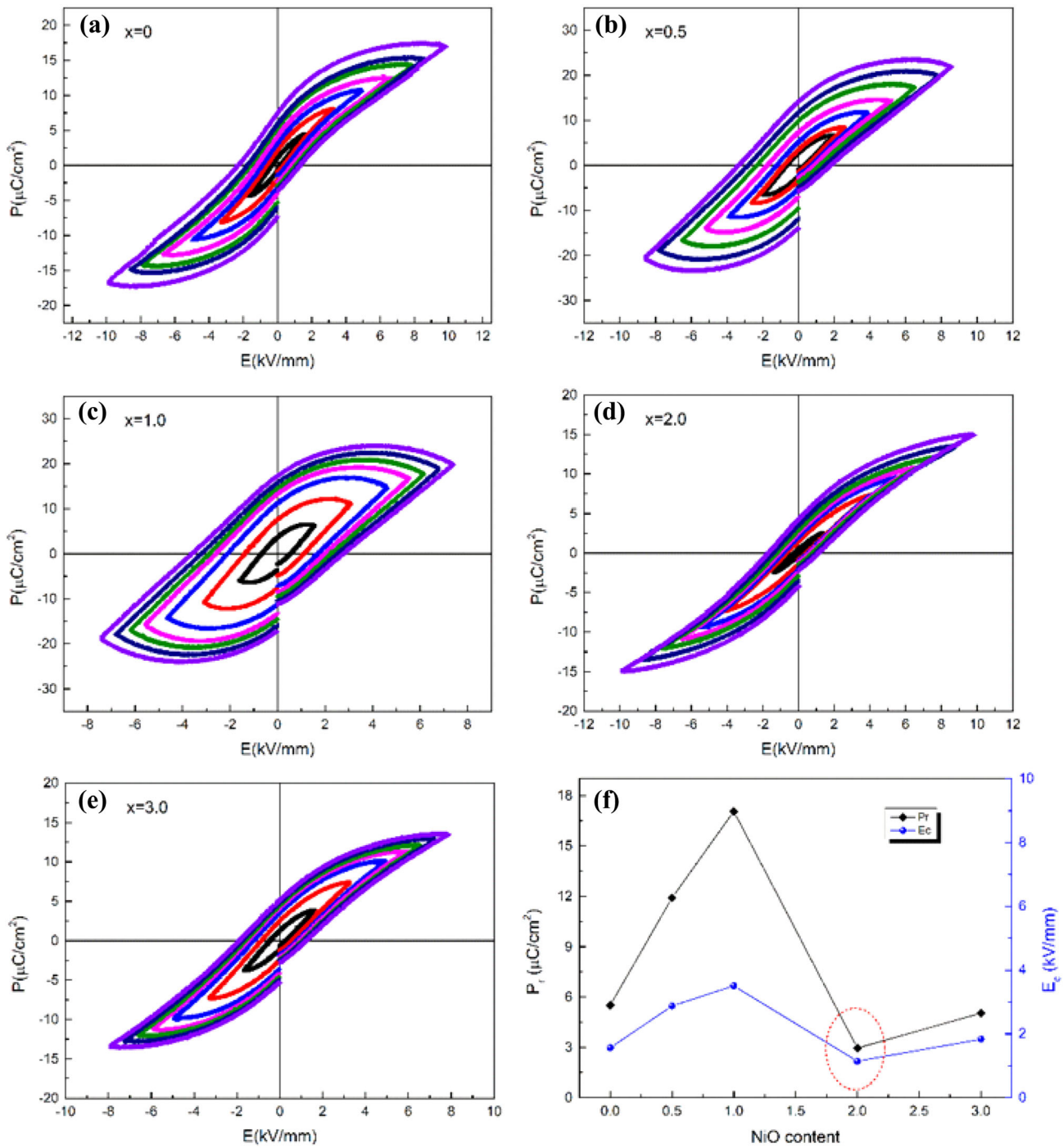

Fig. 3 **a**–**e** P-E loops of $BaTiO_3$-4 mol%Nb_2O_5-xmol%NiO ceramics under different electric field and (**f**) P_r and E_c under 8 kV/mm

[11]. The modified Curie–Weiss law is used to evaluate the dielectric dispersion [12]: $1/\varepsilon - 1/\varepsilon_m = (T - T_m)^{\gamma} / C$, where ε and ε_m are the permittivity and maximum permittivity, respectively; γ is the indicator of the relaxor degree; C is the Curie–Weiss constant. $\gamma = 1$ reflects the ideal ferroelectrics while $\gamma = 2$ represents the excellent relaxor characteristic. The fitted values of γ for BT-Nb-xNiO ceramics at 1 kHz are shown in Fig. 5. For the composition $x = 0$, γ value was calculated to be 1.60, demonstrating the relaxor ferroelectric feature of the BT-Nb ceramics. For the samples with low NiO content ($x = 0.5$–1.0), γ slightly dropped. For the

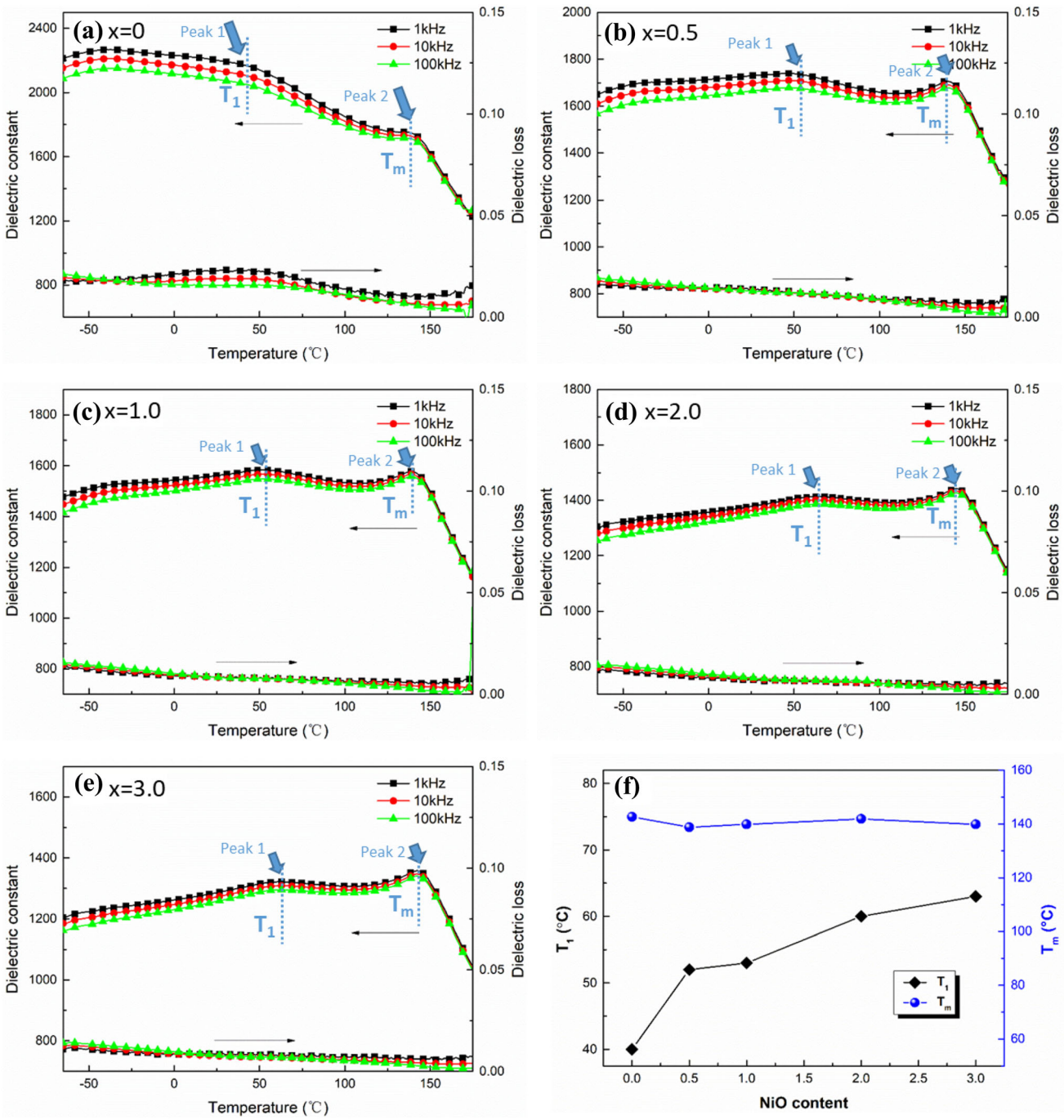

Fig. 4 Frequency and temperature dependence of the dielectric constant and dielectric loss of $BaTiO_3$-4 mol%Nb_2O_5-xmol%NiO ceramics with **a** $x = 0$, **b** $x = 0.5$, **c** $x = 1.0$, **d** $x = 2.0$, **e** $x = 3.0$ and **f** variation of T_1 and T_m

samples with higher NiO content (x = 2.0–3.0), γ increased to 1.78 ~ 1.84. NiO-addition first reduced and then enhanced the relaxor behaviour, which was consistent with the above ferroelectric hysteresis loops analysis. It is believed that in BT-Nb-xNi (x = 0–1.0) ceramics, the degree of long range ferroelectric order is still relatively high although they exhibit relaxor characteristics. After the addition of large content NiO (x = 2.0–3.0), the long range interactions would be destroyed and polar regions forms due to the substitution of Ni^{2+} and Nb^{5+} at B-sites. This enhances compositional fluctuation and structural disorder in the arrangement of cations, leading to the increase in the relaxor degree [13].

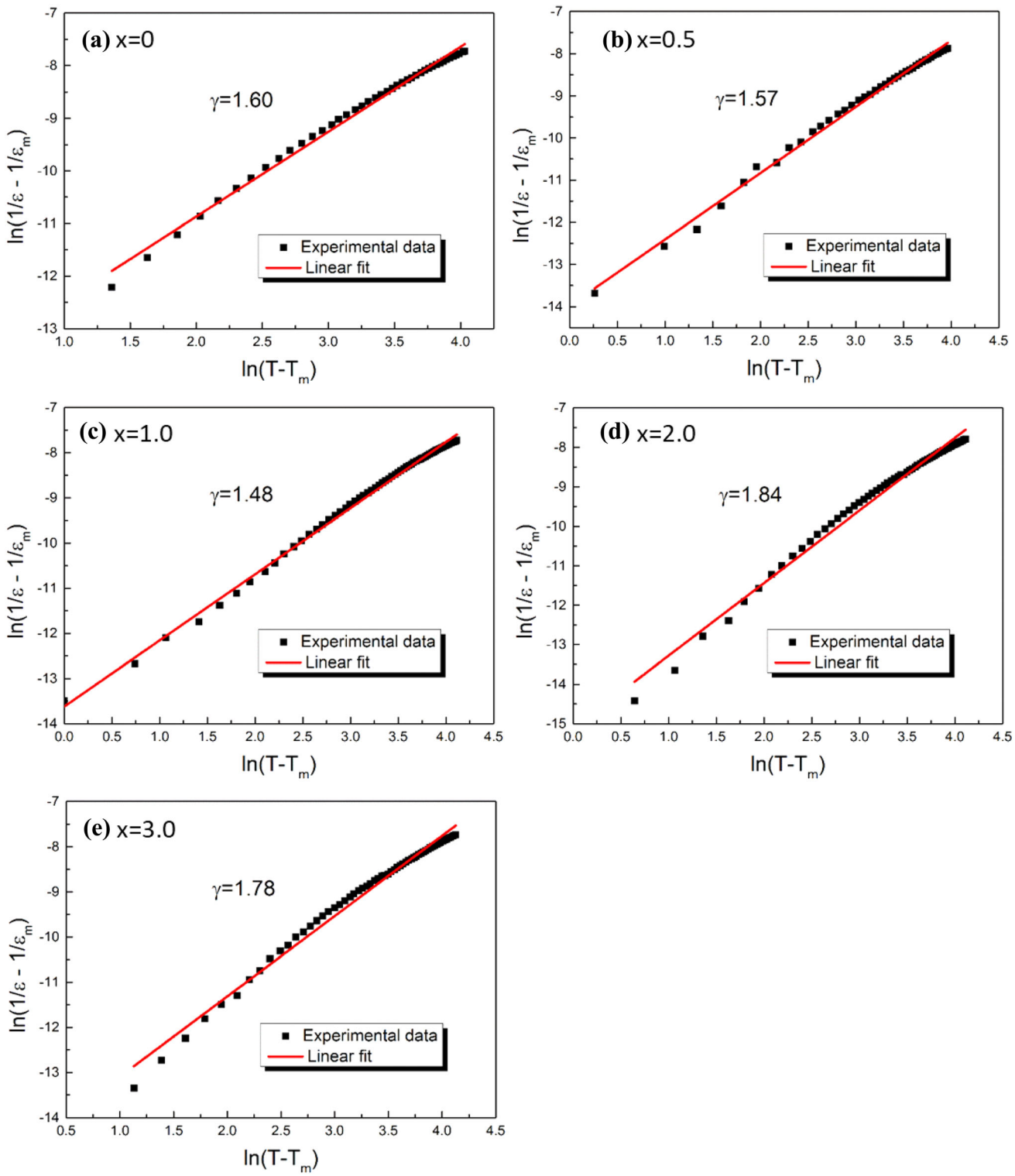

Fig. 5 Plots of $\ln(1/\varepsilon–1/\varepsilon_m)$ versus $\ln(T—T_m)$ at 1 kHz

Figure 6 shows the temperature dependence of dielectric constant and dielectric loss of BT-Nb-xNi ceramics measured from -70 °C to 200 °C at 1 kHz. It was obvious that the permittivity of the system decreased as a whole with NiO adding. The permittivity (ε_r) at room temperature dropped from 2200 in

$x = 0$ to 1285 in $x = 3.0$. The dielectric loss (tanδ) slightly decreased as well with NiO addition. In the composition $x = 1.0$–3.0, the tanδ values at room temperature and 1 kHz were all below 1.00%.

With NiO doping amount increased, the ε_r-T curves of BT-Nb-xNiO system were significantly flattened, leading to greatly optimized dielectric temperature stability. The temperature coefficient of capacitance ($\triangle C/C_{25°C}$) based on room temperature (25 °C) was adopted to evaluate the temperature stability in this paper: $\triangle C/C_{25°C} = (C_T\text{-}C_{25°C})/C_{25°C}$. Figure 7 shows the temperature dependence of $\triangle C/C_{25°C}$ for BT-Nb-xNiO ceramics, in which the rectangular shadow represents the reference range satisfying EIA-X8R specification (− 55–150 °C, $\triangle C/C_{25°C} \leq \pm 15\%$). With proper NiO doping ($x = 0.5$–3.0), the BT-Nb-Ni system can meet X8R criterion (see in Table 2). The optimum NiO doping content was found to be 2.0%, where the dielectric constant and dielectric loss at room temperature was 1380 and 0.71%, with $\triangle C/C_{25°C} \leq \pm 15\%$ in the temperature range of − 65–170 °C. The results were also compared with other BT-based systems reported in literatures [14–16]. Although the permittivity of BT-Nb-2.0%Ni was slightly lower than that of other compositions reported in literatures, it possessed a wider temperature range with stable permittivity. In addition, the electric resistivity of all the samples were above 10^{12} Ω·cm, indicating favorable insulativity. Therefore, BT-Nb-2.0%Ni could be a promising material used for MLCC dielectrics.

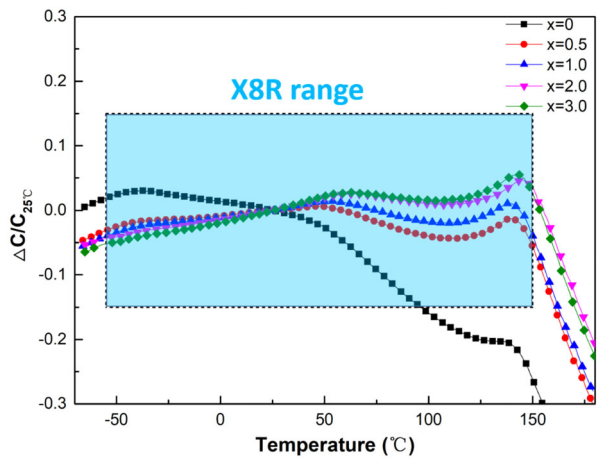

Fig. 7 The temperature variation of capacitance of $BaTiO_3$-4 mol%Nb_2O_5-xmol%NiO ceramics

4 Conclusion

Ni addition was found to greatly optimize the dielectric temperature stability of BT-Nb system. With proper NiO doping ($x = 0.5$–3.0), the BT-Nb-Ni system can meet X8R criterion. The optimum dielectric property was achieved in the composition $x = 2.0$, at which the dielectric constant at room

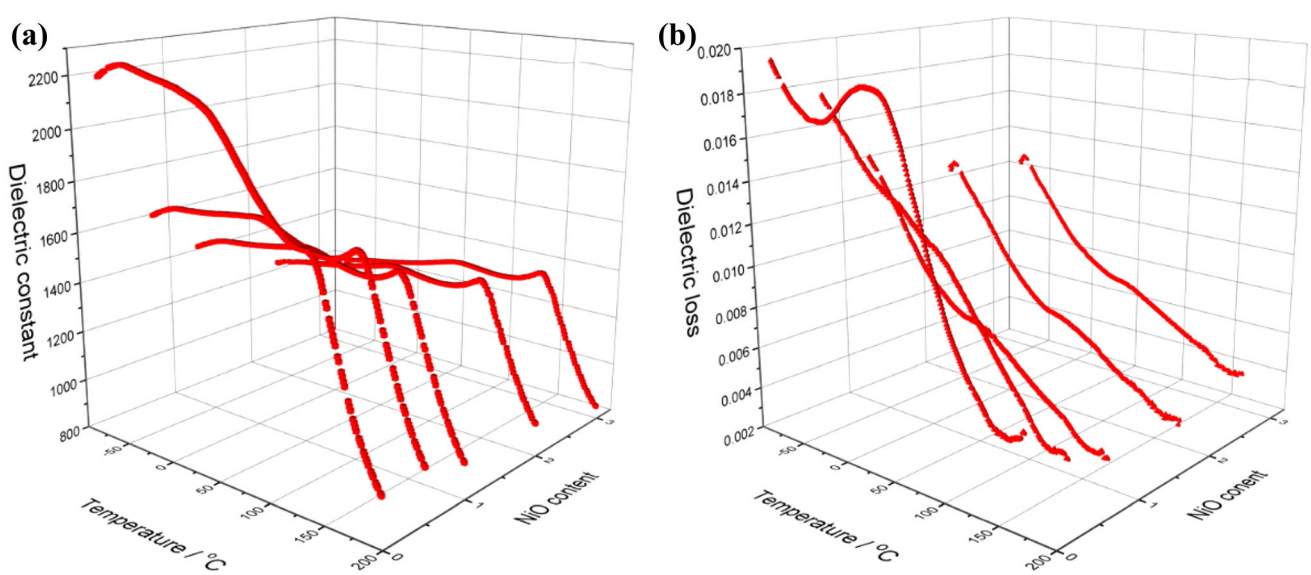

Fig. 6 Temperature dependence of (**a**) dielectric constant and (**b**) dielectric loss of $BaTiO_3$-4 mol%Nb_2O_5-xmol%NiO ceramics measured from − 70 to 200 °C at 1 kHz

Table 2 Dielectric properties and resistivity of $BaTiO_3$-4 mol%Nb_2O_5-xmol%NiO ceramics

Composition	ε_r (at 25 °C, 1 kHz)	Tanδ (at 25 °C, 1 kHz) (%)	Temperature range satisfying $\Delta C/C_{25°C} \leq \pm 15\%$ (°C)	Resistivity(Ω·cm) ($\times 10^{12}$)
$x = 0$	2200	2.28	− 65–95	6.77
$x = 0.5$	1730	1.36	− 65–160	1.45
$x = 1.0$	1560	0.86	− 65–162	2.24
$x = 2.0$	1380	0.71	− 65–170	2.21
$x = 3.0$	1285	0.86	− 65–170	1.28

temperature was 1380, with $\triangle C/C_{25°C} \leq \pm 15\%$ in the temperature range of − 65–170 °C.

Acknowledgement

This work was supported by the National Natural Science Foundation of China (No. 51372191), Start-up Grant of Chengdu University of Technology (No. 10900-KYQD-06848), Young and Middle-aged Key Teachers Development Fund of Chengdu University of Technology (No. 10912-JXGG2020-06848), Sichuan Science and Technology Program (No. 2021JDRC0105).

Authors' contributions

QX designed and wrote the manuscript. WH and RD completed some data processing. HC did some of the experiments. HL provided technical support during the study.

Funding

This work was supported by the National Natural Science Foundation of China (No. 51372191), Start-up Grant of Chengdu University of Technology (Grant No. 10900-KYQD-06848), Young and Middle-aged Key Teachers Development Fund of Chengdu University of Technology (No. 10912-JXGG2020-06848).

Data availability

All data and material generated during the study are available.

Declarations

Conflict of interest No conflict of interest exits in the submission of this manuscript.

Consent to participate All the authors consent to participate and submit this manuscript to *Journal of Materials Science: Materials in Electronics*.

Consent for publication All the authors consent for publication of this paper in *Journal of Materials Science: Materials in Electronics*.

Human and animal rights Not applicable

References

1. L. Li, J. Yu, N. Zhang et al., Synthesis and characterization of X8R $BaTiO_3$-based dielectric ceramics by doping with $NiNb_2O_6$ nanopowders[J]. J. Mater. Sci.: Mater. Electron. **26**(12), 9522–9528 (2015)
2. G. Yao, X. Wang, Y. Zhang et al., Nb-modified $0.9BaTiO_3$–$0.1(Bi_{0.5}Na_{0.5})TiO_3$ ceramics for X9R high-temperature dielectrics application prepared by coating method. J. Am. Ceram. Soc. **95**(11), 3525–3531 (2012)
3. Sun Y, Liu H, Hao H, et al. Impedance analysis of Nb_2O_5 doped $BaTiO_3$ -$Na_{0.5}Bi_{0.5}TiO_3$ ceramics[C]. Applications of ferroelectrics, international workshop on acoustic transduction materials and devices & workshop on piezoresponse force microscopy, 2014: 1–5.
4. G. Yao, X. Wang, Y. Wu et al., Nb-doped $0.9BaTiO_3$–$0.1(Bi_{0.5}Na_{0.5})TiO_3$ ceramics with stable dielectric properties at high temperature[J]. J. Am. Ceram. Soc. **95**(2), 614–618 (2012)
5. Y. Liu, B. Cui, Y. Wang et al., Core-shell structure and dielectric properties of $Ba_{0.991}Bi_{0.006}TiO_3$@$Nb_2O_5$-$Co_3O_4$ ceramics. J. Am. Ceram. Soc. **99**(5), 1664–1670 (2016)

6. B. Xiong, H. Hao, S. Zhang et al., Dielectric behaviors of Nb_2O_5–Co_2O_3 doped $BaTiO_3$–$Bi(Mg_{1/2}Ti_{1/2})O_3$ ceramics[J]. Ceram. Int. **38**, S45–S48 (2012)
7. L. Li, J. Chen, D. Guo et al., An ultra-broad working temperature dielectric material obtained with Praseodymium doped $BaTiO_3$–$(Bi_{0.5}Na_{0.5})TiO_3$–Nb_2O_5 based ceramics[J]. Ceram. Int. **40**(8), 12539–12543 (2014)
8. S. Wang, S. Zhang, X. Zhou et al., Investigation on dielectric properties of $BaTiO_3$ co-doped with Ni and Nb[J]. Mater. Lett. **60**, 909–911 (2006)
9. L. Li, R. Fu, Q. Liao et al., Doping behaviors of NiO and Nb_2O_5 in $BaTiO_3$ and dielectric properties of $BaTiO_3$-based X7R ceramics[J]. Ceram. Int. **38**(3), 1915–1920 (2012)
10. M. Kahn, Influence of grain growth on dielectric properties of Nb-doped $BaTiO_3$[J]. J. Am. Ceram. Soc. **54**(9), 455–457 (1971)
11. Z. Dai, J. Xie, X. Fan et al., Enhanced energy storage properties and stability of $Sr(Sc_{0.5}Nb_{0.5})O_3$ modified $0.65BaTiO_3$–$0.35Bi_{0.5}Na_{0.5}TiO_3$ ceramics[J]. Chem. Eng. J **397**, 125520 (2020)
12. P. Zhao, B. Tang, Z. Fang et al., Improved dielectric breakdown strength and energy storage properties in Er_2O_3 modified $Sr_{0.35}Bi_{0.35}K_{0.25}TiO_3$[J]. Chem. Eng. J. **403**, 126290 (2021)
13. P. Zhao, B. Tang, Z. Fang et al., Structure, dielectric and relaxor properties of $Sr_{0.7}Bi_{0.2T}iO_3$-$K_{0.5}Bi_{0.5}TiO_3$ lead-free ceramics for energy storage applications[J]. J. Materiom. **7**, 195–207 (2021)
14. Z. Tian, X. Wang, Y. Zhang et al., Formation of core-shell structure in ultrafine-grained $BaTiO_3$-based ceramics through nanodopant method[J]. J. Am. Ceram. Soc. **93**(1), 171–175 (2010)
15. Z. Tian, X. Wang, H. Gong et al., Core–shell structure in nanocrystalline modified $BaTiO_3$ dielectric ceramics prepared by different sintering methods[J]. J. Am. Ceram. Soc. **94**(4), 973–977 (2011)
16. D. Ma, X. Chen, G. Huang et al., Temperature stability, structural evolution and dielectric properties of $BaTiO_3$–$Bi(Mg_{2/3}Ta_{1/3})O_3$ perovskite ceramics[J]. Ceram. Int. **41**(5), 7157–7161 (2015)